
Article:
Fernández Silva, B., Kawalko, J. orcid.org/0000-0001-5469-2338, Muszka, K. orcid.org/0000-0001-8449-7795 et al. (3 more authors) (2022) Deformation modes investigation during ex-situ dwell fatigue testing in a bimodal near-α titanium alloy. International Journal of Fatigue, 163. 107098. ISSN: 0142-1123

https://doi.org/10.1016/j.ijfatigue.2022.107098

International Journal of Fatigue 163 (2022) 107098

Contents lists available at ScienceDirect

International Journal of Fatigue

journal homepage: www.elsevier.com/locate/ijfatigue

Deformation modes investigation during ex-situ dwell fatigue testing in a bimodal near-α titanium alloy

B. Fernández Silva [a,*], J. Kawalko [b], K. Muszka [b], M. Jackson [a], K. Fox [c], B.P. Wynne [a,d]

[a] Department of Material Science and Engineering, The University of Sheffield, Sheffield S1 3JD, UK
[b] AGH University of Science and Technology, al. Mickiewicza 30, 30-059 Kraków, Poland
[c] Rolls-Royce plc, P.O. Box 31, Derby DE24 8BJ, UK
[d] Department of Mechanical and Aerospace Engineering, The University of Strathclyde, 75 Montrose St, Glasgow G1 1XJ, UK

ARTICLE INFO

Keywords:
Dwell fatigue
Titanium alloys
Faceting
Slip
Twinning

ABSTRACT

In this paper, quasi-cleavage facet formation and deformation mechanisms in dwell fatigue have been studied on specimens from a Ti834 compressor disc alloy with a bimodal microstructure by ex-situ dwell fatigue testing at temperatures between 80 °C and 200 °C. Basal <a> slip was observed in grains with their c-axis near parallel the loading direction, while colonies similarly oriented accommodate deformation by tensile twins $\{10\bar{1}2\}\langle 11\bar{2}0 >$. This type of slip in basal planes is the most critical damage mode leading to failure during dwell fatigue loading. A Rogue colony-grain combination is presented and a possible criterion for slip transfer in bimodal titanium alloys is introduced. The requirements cited for quasi-cleavage facet formation leading to dwell fatigue failure have been experimentally observed in agreement with the suggested hypothesis in previously presented crystal plasticity models.

1. Introduction

Near-α and α + β titanium alloys are susceptible to reductions in fatigue life when exposed to relatively high constant dwell stress during the loading cycle [1–4]. This reduction in fatigue life occurs when cycling at temperatures up to 200 °C and is known as cold dwell fatigue [5]. The fracture surface is characterised by regions of sub-surface quasi-cleavage facets that are near perpendicular to the primary loading direction, which are commonly found near the failure initiation sites [6–8]. The facets also appear to have a microstructure basis being directly related to clusters of similarly orientated primary α (α_p) grains, known as macrozones, that have their basal planes near normal to the loading direction [9,10].

The mechanism for crack initiation under dwell conditions has been proposed by the modified Stroh Pile up model, where a certain neighboring grain combination needs to exist, i.e., a 'soft' grain neighboring a 'hard' grain, which are favorably and unfavorably orientated for slip, respectively [11,12]. This combination leads to a dislocation pile up on the soft side of their boundary, inducing shear stress and therefore slip in the hard grain, which in conjunction with the applied cyclic stress nucleates a fatigue crack subsurface. Cold creep has also been identified as an additional requirement for crack initiation by a phenomenon known as load-shedding [13]. During dwelling, stress relaxation within the soft grain due to the rate-dependent slip accumulation combined with the strain compatibility requirements at the boundary induces even higher stresses into the hard grain. This effect of load shedding under stress-controlled experiments has been widely utilised to explain the dwell fatigue failure mechanisms for to quasi-cleavage facet formation [5,14–16]. Crystal plasticity modelling has also shown that a soft grain having a c-axis near normal to the loading direction with an active prismatic slip plane at an angle of about 70° to the normal to loading neighbouring a hard grain having its c-axis near parallel to loading direction is the most damaging combination. This combination is known as the Rogue combination [17]. Modelling has also suggested that localised accumulated slip in the soft grain is further exacerbated if the grain boundary is parallel to an active slip system in that grain [18]. Experimental validation is limited at the grain scale level, however; faceted initiation sites have been associated with hard regions that have neighbouring soft regions, which is consistent with the model concepts presented above [9,14].

A temperature of 120 °C has been established as the worst-case scenario for dwell debit by both full-scale testing and crystal plasticity modelling in the alloys considered [5,19]. However, previous studies considered the dwell-temperature fatigue susceptibility to be alloy

* Corresponding author.
E-mail address: b.silva@sheffield.ac.uk (B. Fernández Silva).

https://doi.org/10.1016/j.ijfatigue.2022.107098
Received 22 March 2022; Received in revised form 31 May 2022; Accepted 22 June 2022
Available online 25 June 2022

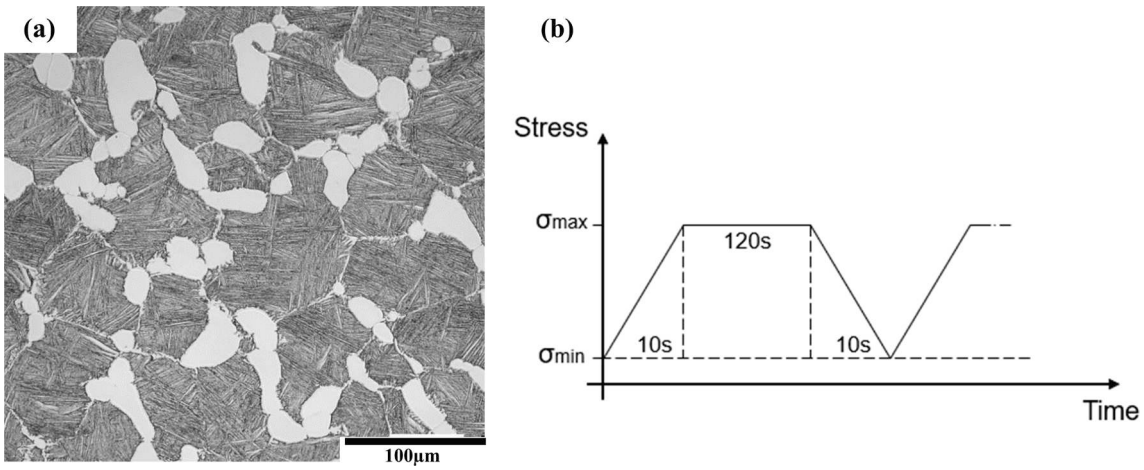

Fig. 1. (a) Optical micrograph of Ti834 bimodal microstructure with 25% α_p and (b) schematic trapezoidal waveform curve for dwell fatigue experiment.

Table 1
Semi quantitative EDS composition analysis of α_p grain, α_s colony and the base material.

Location	Ti	Al	Sn	Zr	Nb	Mo	Si
Overall material	86.31	4.70	3.99	3.52	0.63	0.51	0.34
αp grain	86.52	5.72	3.78	3.06	0.51	0.10	0.31
αs colony	85.57	4.71	4.20	3.68	0.92	0.72	0.31

All elements are specified in weight percent.

dependent [20]. At this temperature, the relative creep slip rate in the soft grain during the dwell is at its highest relative rate compared to the hard grain, producing the strongest load shedding between the hard and soft grain [19]. At higher temperatures the dwell effect is reduced because of the presence of more activated slip systems [19,21] and an decrease of strain rate sensitivity [22,23]. More slip systems lead to less anisotropy between the hard and soft grains reducing the stress mismatch across the boundary, decrease in strain rate sensitivity leads to less creep strain accumulation in the soft grain during the dwell, reducing the magnitude of the peak stresses in the hard grain. This phenomenon is known as thermal alleviation and reduces the dwell fatigue sensitivity in titanium alloys [23,24].

The bulk of the experimental research on dwell fatigue analysis mentioned above has been focused on room temperature testing using materials with a large volume fraction of α_p. Here, the deformation modes of a more realistic in-service bimodal microstructure of 25% α_p grains in a matrix of secondary α (α_s) colonies subjected to dwell fatigue are assessed by a combination of EBSD and dwell fatigue testing at temperatures in the range that are most detrimental for dwell debit. The alloy used is near-α Ti834, which has a temperature capability up to 600 °C and is used almost exclusively in the high-pressure section of jet turbine engines where a balance of good fatigue and creep properties at high temperatures is required [25]. The main objective is to understand how deformation in favourably and unfavourably orientated grains for slip is accommodated as a function of temperature. A study of the active deformation modes by slip trace analysis was carried out on α_p grains and α_s colonies with an emphasis on slip transfer analysis. An extensive investigation was carried out to understand the crystallographic interactions that are required for slip transfer under dwell fatigue conditions. Validation of the crystal plasticity modelling mentioned previously [14,18] is accomplished at the grain scale level.

2. Experimental

Ti834 with a bimodal microstructure was provided by Rolls-Royce plc for this work from a high-pressure compressor disc. The microstructure contained 25% α_p within a transformed beta matrix of α_s colonies, as shown in Fig. 1(a). The average α_p and α_s colony size was 25 μm and 50 μm, respectively. The bulk composition analysis is summarised in Table 1 as well as the independent compositions of α_p grains and α_s colonies.

Flat 2 mm thick dog-bone specimens with a gauge length of 3 mm gauge and width of 2 mm were electrical discharge machined (EDM) from the as-received material and lightly machined to remove the re-melt EDM layer. To remove the subsurface damage because of the machining and achieve a mirror surface finishing for EBSD analysis the specimens were ground with SiC paper from 400 to 4000 grit size and polished for 15 min with Colloidal silica 0.05 μm and 10 %H_2O_2.

Specimens were dwell fatigue tested at 80 °C, 120 °C, 150 °C and 200 °C following a trapezoidal wave form loading with a maximum applied stress of 850 MPa (90% of the room temperature yield strength), R = 0.1, a dwell period of 120 s, and a load/unload period of 10 s (Fig. 1 (b)). These conditions were chosen in order to make the specimens susceptible to dwell fatigue failure before reaching 500 cycles [6,9,26,27]. The load at peak stress was chosen to be the same regardless of the testing temperature as the focus was on understanding the impact of dwell at different temperatures that may be experienced in service [23]. Dwell fatigue tests were performed using a 5kN Kammrath & Weiss tensile stage with heater module in a FEI Versa 3D SEM equipped with an EDAX Hikari EBSD camera and TSL OIM system for EBSD data collection. All samples were tested up to 550 cycles. The dwell experiment was interrupted, and samples unloaded and cooled down after 50 and 550 cycles to collect SEM images and EBSD for ex-situ investigation.

Orientation image maps (OIMs) were acquired at the gauge area before testing and high resolution OIMs were collected after 550 cycles at the centre of the gauge length for each test temperature covering areas of 400x400 μm^2 with a step size of 0.6 μm. Secondary Electron (SE) and Backscattered images (BSE) from each region were taken for a precise distinction between α_p grains and α_s colonies. This allowed for a clear observation of slip bands on the surface of the deformed samples as well as to differentiate microstructure features. Slip band characterisation was undertaken at 50 and 550 cycles for each temperature. The theoretical slip traces were calculated by using the orientation data of each individual grains using a Crystal Mathematics Tool (developed by The University of Sheffield Materials Department). The slip systems considered include basal < a> (Ba), prismatic < a> (Pr), 1st order pyramidal <a> and <c+a> (1st Py), and 2nd order pyramidal <c+a> slip (2nd Py). A general 1st order pyramidal slip is used as the slip trace analysis cannot distinguish between first order <a> and <c+a> pyramidal slip. The traces were then compared with the experimental slip band observations and an angle matching criterion of ±5° was used to determine the likely slip system as it was found to be the best value to

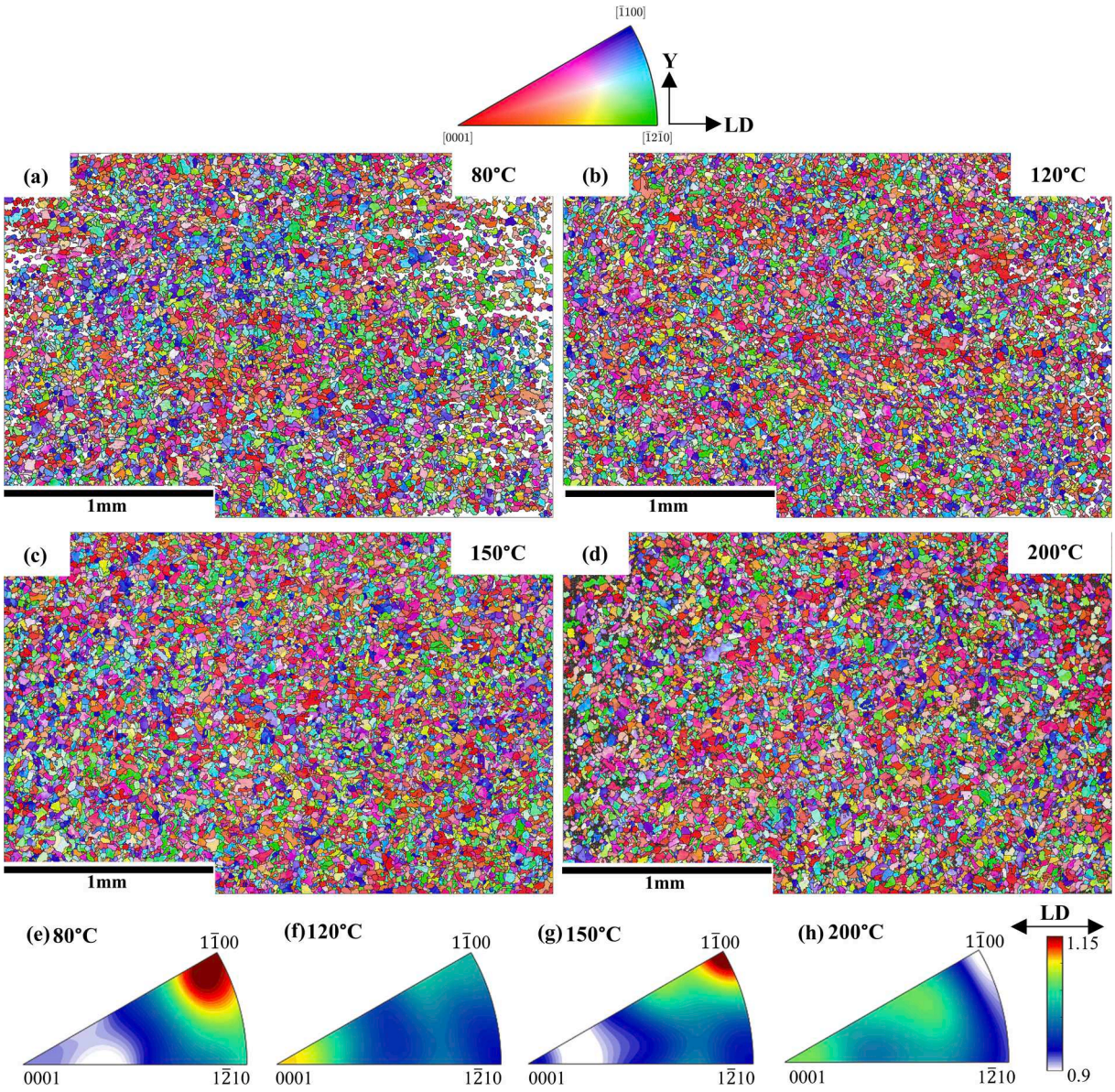

Fig. 2. Low Resolution IPF-LD orientation maps of the gauge area from each specimen (a-d) and inverse pole figure plot (e-h) regarding the loading direction.

maximize unique slip solution and minimised multiple solutions in predicting a slip system [28]. Each experimental slip band was characterized by finding the theoretical trace with the closest match. When more than one solution is observed the trace with the highest Schmid factor is considered.

3. Results and discussion

3.1. Initial texture

The large scale OIMs, using inverse pole figure (IPF) colouring relative to the loading direction (LD), and inverse pole figures of each of the test specimens prior to heating and fatigue testing are presented in Fig. 2. Unless otherwise indicated, this is the colour key of all IPF orientation maps in this work. The LD axis is parallel to the loading direction and the Y axis is perpendicular to LD on the gauge area plane of the dog bone specimens. All OIMs (Fig. 2(a-d)) show no significant evidence of agglomeration of similarly orientated grains/colonies which would lead to macrozones of millimetres in length as commonly observed commonly observed in titanium mill products in near-α and α + β titanium alloys that can reach mm in length [3,29–32]. The crystallographic textures are also very weak, with a maximum intensity of 1.3 times random. Specimens that were to be tested at 80 °C (Fig. 2(e)) and 150 °C (Fig. 2(g)) displayed a slightly greater level of {1$\bar{1}$00} planes perpendicular to the loading direction, while a slight increase in {0001} planes perpendicular to the loading direction is present in the 120 °C (Fig. 2(f)) and 200 °C specimens (Fig. 2(h)). This meant that the 120 °C and 200 °C test specimens had a slightly higher density of hard grains/colonies, whilst the 80 °C and 150 °C test specimens contained a slightly higher volume fraction of grains/colonies orientated for relatively easy slip.

3.2. Deformation behaviour

All ex-situ test specimens survived to 550 cycles with total plastic strain levels between 1% and 9% but with no evidence of surface fatigue crack initiation. The stress–strain responses for the first loading cycle are presented in Fig. 3(a) and the total permanent strains as a function of testing time are presented in Fig. 3(b). The first loading cycle stress–-strain response for all specimens consisted of elastic loading with some

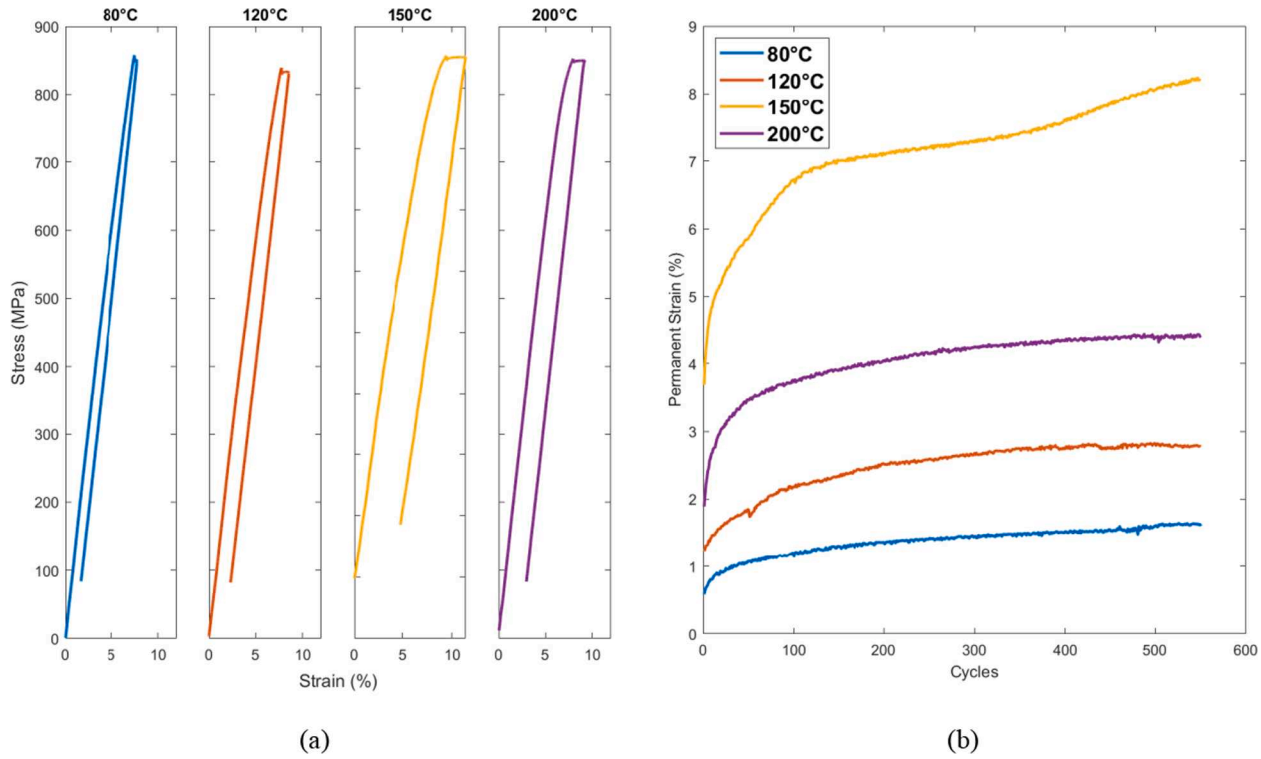

Fig. 3. (a) Stress-Strain curve after 1 dwell fatigue cycle (note, there was no evidence of tensile specimen slippage in any of the tests) and (b) permanent strain at each temperature during dwell at each temperature.

level of deviation from linearity prior to reaching the peak stress, whereupon all the specimens increased their elongation under constant load before unloading. From the stress–strain response of the first cycle, Fig. 3(a), the yield strength 650 MPa for the samples tested at 80 °C, 120 °C and 200 °C and 400 MPa for the 150 °C specimen. It can be noticed that the creep strain increased with increasing temperature, Fig. 3(b), but there was an anomaly with the 150 °C specimen, which had a greater level of creep strain than the specimen tested at 200 °C. Furthermore, the 150 °C specimen upon loading deviated from elastic linearity at a lower stress than all other samples, suggesting the slightly higher volume fraction of soft orientated grains within this specimen (Fig. 2(g)) at this test temperature was sufficient to reduce the yield stress and enable a higher creep rate. The accumulated plastic strain as a function of testing time shows a similar trend with the 150 °C specimen having a higher rate of creep in the early cycling stages (Fig. 3 (b)). Afterwards, and as for all specimens, the rate of elongation is significantly reduced. However, the creep rate did begin to increase for 150 °C specimen towards the end of the test, whereas the others maintained a relatively low creep rate. The permanent strain at the end of testing the 150 °C specimen has almost doubled the strain achieved by the 200 °C specimen.

Fig. 4 (a,d,g,j) show high resolution IPF orientation maps for each sample before testing, at 0 cycles. These maps cover areas that are representative to the overall texture previously mentioned in Fig. 2. The surface relief of the same area after 550 cycles is displayed in Fig. 4 (b,e, h,k) using SE and the microstructure after 550 cycles is shown in Fig. 4 (c,f,i,l) using BSE, where the αp grains and αs colonies are easily distinguished. All regions have a weak texture with no obvious orientation clustering, with the hard-orientated regions being mainly αp grains in areas shown. For all testing temperatures, the slip traces occurred randomly within the microstructure, with no clear preference for αp grains or αs colonies, except for hard orientated αp grains and αs colonies where no deformation was observed (Fig. 4 (b,e,h,k)). However, the number of slip traces is higher at temperatures of 150 °C and 200 °C, while much less slip is observed at 80 °C. The surface relief on the 150 °C specimen is also noticeably higher than for the 200 °C specimen, confirming that the specimen tested at 150 °C experiences greater strain than the 200 °C specimen.

In agreement with previous studies, a significant level of plastic deformation takes place in the early cycling stages, Fig. 3(a), in particular the first cycle [33,34]. The accumulated permanent strain increases for the higher temperatures tested, suggesting that cyclic dwell creep resistance decreases with increasing temperature for Ti834, as was observed for Ti64 [35]. However, the anomaly observed at the 150 °C specimen with a higher strain than 200 °C specimen suggests that the soft texture in the specimen plays a role in creep behaviour. Such variation in creep behaviour was previously observed by Li *et al.* [36] and Barkia *et al.* [37] when a higher creep rate was showed when loading parallel to the rolling direction. However, further testing is required at this temperature with a stronger texture to conclude the effect of texture on creep within the current investigation.

3.3. Deformation by slip

For all testing temperatures, the slip traces occurred randomly within the microstructure, with no clear preference for α_p grains or α_s colonies, except for hard orientated α_p grains and α_s colonies where no deformation was initially observed. Contrastingly, other studies showed a tendency for initial slip on α_p grains at early stages during the deformation at the proof stress [26,38,39]. However, the number of slip traces observed increases steadily with temperature for the areas analysed with significant low slip occurrences at 80 °C.

Fig. 5 summarises the slip trace analysis for specimens tested to 550 cycles. The bar plot colours represent the percentage of α_p grains that have no evidence of slip or contain a specific slip trace, while each bar represents a different testing temperature. A similarly detailed slip analysis was also carried out for 50 cycles and no significant differences in slip trace distribution were observed in comparison with the results at 550 cycles. The main difference being that the total number of slip traces within the same grain or colony increases at the higher cycles. The only

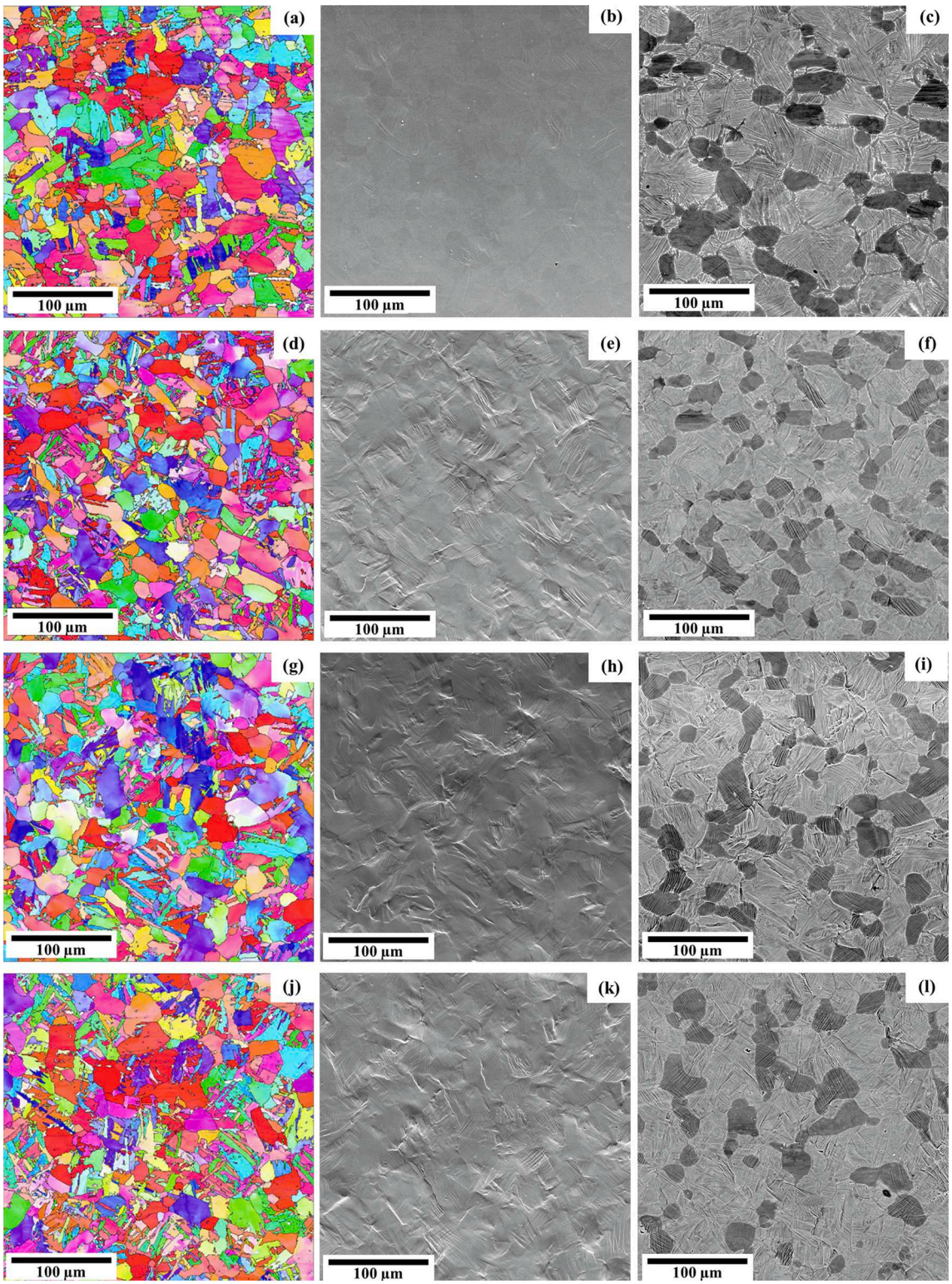

Fig. 4. High resolution images from a central location of each sample showing: (a,d,g,j) High-Resolution IPF-LD orientation maps regarding the loading direction before cycling, (b,e,h,k) SE images and (c,f,i,l) BSE after 550 cycles displaying the surface relief and bimodal microstructure. Note: Fig. 4(c) displays a different location from (a) and (b). Loading is applied in the horizontal axis.

evidence of any new slip system activity was that a few harder orientated basal grains contained <a> slip traces at 150 °C and 200 °C.

No matter the temperature considered <a> type slip governs the deformation with a high density of basal <a> slip except for the 80 °C specimen. The preference for <a> type slip increases with temperature as well as the density of basal <a> slip except for the 80 °C specimen. At 80 °C close to 40% of the α_p grains show active slip with only 2% being basal <a> slip while for the higher temperatures, there was a significant increase in the number of α_p grains (>80%) exhibiting slip. Above 80 °C, the active α_p grains contained mostly <a> type slip. However, at 120 °C and 200 °C close to 50% of the <a> type slip was basal, while for 150 °C 31% of the <a> type slip was basal matching the prismatic <a> slip.

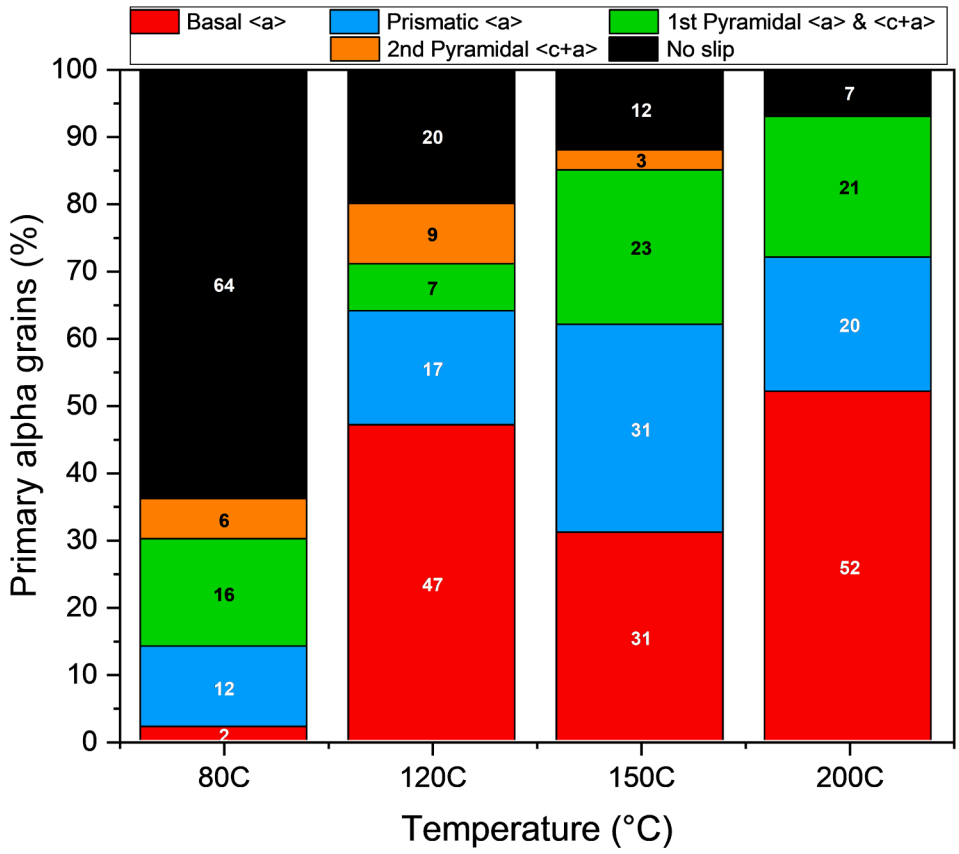

Fig. 5. Slip analysis on α_p grains as a function of temperature after 550 cycles.

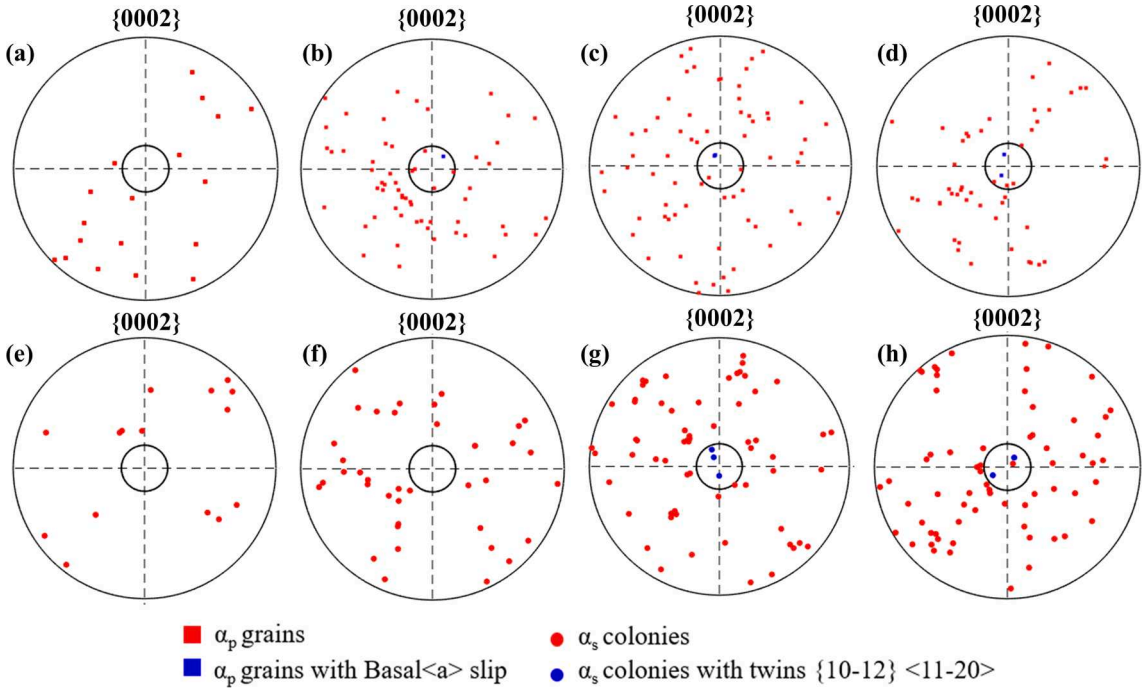

Fig. 6. Basal {0 0 0 2} pole figures of the individual orientation from α_p grains (top) and α_s colonies (bottom) with active slip from temperature (a,e) 80 °C, (b,f) 120 °C, (c,g) 150 °C and (d,h) 200 °C respectively with the loading axis in the centre. α_p grains with basal slip and α_s colonies with tensile twins are highlighted in blue. The black circle in the centre indicates a 20° inclination of the c-axis regarding the loading direction.

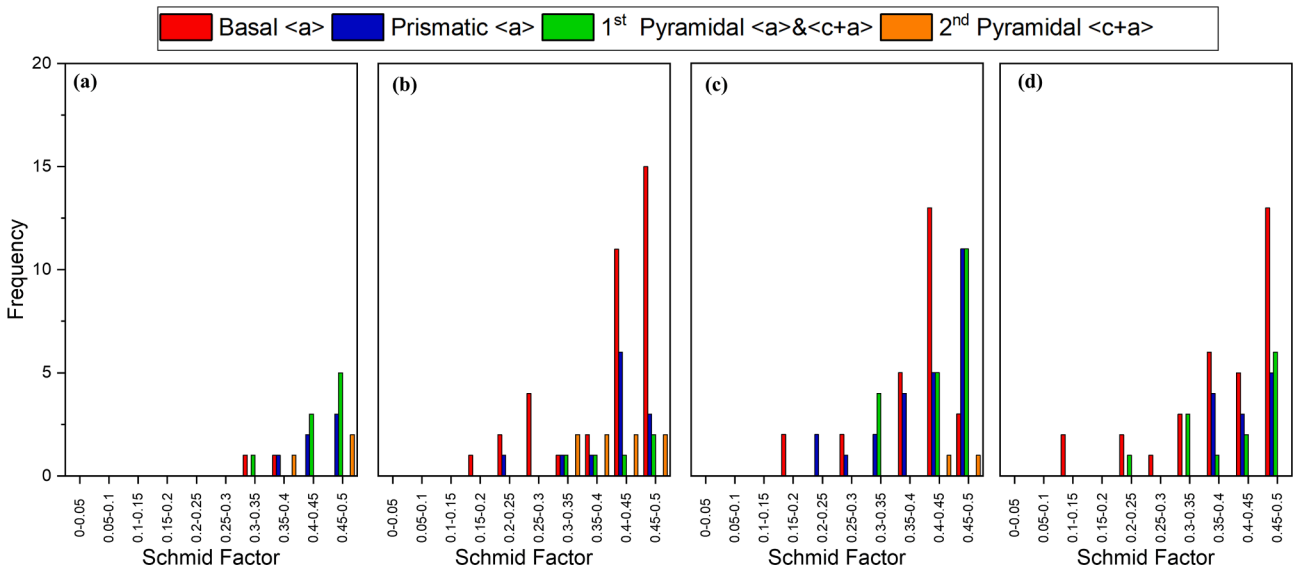

Fig. 7. Schmid factor analysis on primary alpha grains after 550 cycles at (a) 80 °C, (b) 120 °C, (c) 150 °C and (d) 200 °C.

The overall Schmid Factor for basal slip in each sample is similar suggesting that the low number of active basal slip at 80 °C is due to the temperature dependence of the Critical Resolved Shear Stress (CRSS) rather than the influence of texture. However, the Schmid Factor values for prismatic <a> were higher for the 150 °C specimen suggesting the influence of the softer texture observed in this sample.

Deformation pattern appears to stabilise at the early stages of cycling as there was no significant change in slip trace type within individual grains or colonies from 50 to 550 cycles, as previously reported [40]. However, there was an increase in slip trace density with increasing number of cycles. Similar to previous studies, basal and prismatic <a> type of slips are predominant in α_p grains under dwell fatigue conditions in Ti64 [41] and Ti6242 [42]. Most research reports that dwell fatigue facets were found in grains with their c-axis between 10° and 30° from the loading axis with no presence of twins, neither in grains nor in colonies [7,8]. In this study, slip in grains occurs from declination values of 5° from the loading axis. Fig. 6 shows grains with active basal <a> slip. It can be noticed that basal slip occurred in grain with their c-axis between 5° to 70° from the loading direction.

The individual orientations of each α_p grain and α_s colony with active slip are plotted in the Basal {0002} pole figures in Fig. 6. A wide range of orientation are covered by both α_p grains and α_s colonies suggesting a balanced representation of the different crystallographic orientation domains leading to the wide variety of slip active systems as observed in Fig. 5 for the analysis on α_p grains. Except for the lowest temperature, 80 °C, a few hard α_p grains with their c-axis orientated below 20° from loading direction showed active slip. In particular, one hard α_p grain at 120 °C and two hard α_p grains at 150 °C and 200 °C showed Basal <a> slip, Fig. 6(b-d). Although not deeply investigated in this work, deformation by slip in colonies was observed only with a c-axis declination above 20° while deformation by twinning occurs at c-axis between 10° and 20°. Several occurrences were found at the 150 °C and 200 °C specimens (Fig. 6(g,h)). These results are in accordance with tensile twins observed in Ti64 at room temperature under dwell fatigue conditions [43,44]. Note however that tensile twins were observed in failed specimens of other full-scale tests from the same Ti834 compressor disc material at testing temperatures like the current investigation: 80 °C, 120 °C, 150 °C and 250 °C. These tensile twins were observed in most of the hard α_s colonies present in a larger area analysed just below the fracture surface (4 × 0.5 mm^2). The twin density appeared to be closely related to the density of hard orientated α_s colonies at each area investigated suggesting no temperature dependence for twin formation.

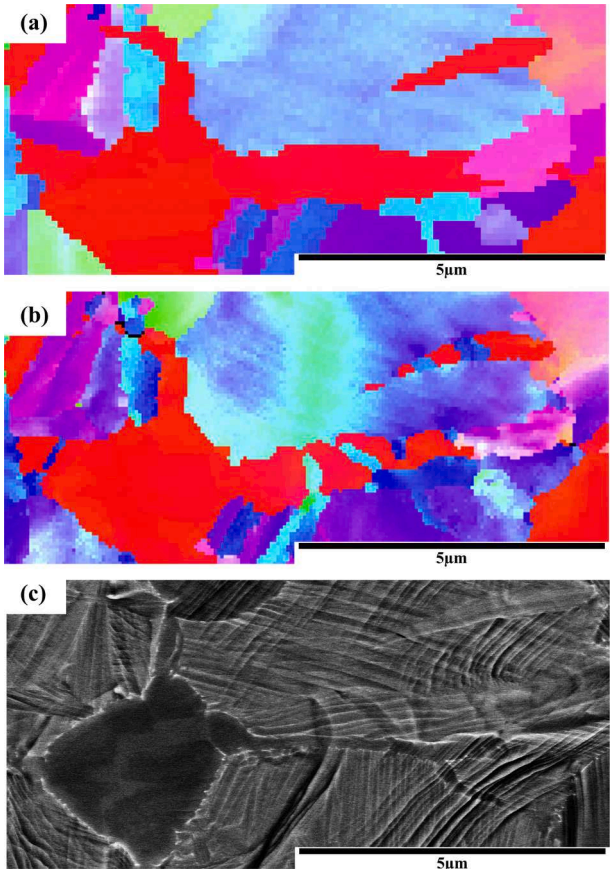

Fig. 8. IPF-LD map of hard and soft α_s colonies surrounding a α_p hard grain at (a) cycles, (b) after 550 cycles at 150 °C displaying deformation by twinning in the hard colony and (c) BSE equivalent image showing the bimodal microstructure.

The Schmid Factor, m, analysis for actively deforming α_p grains at 550 cycles was obtained from the slip trace analysis for each slip system is summarised in Fig. 7. For most of the grains, the Schmid factor of the active slip system is relatively high, being above 0.30. However, at the higher temperatures of 120 °C (Fig. 7 (b), 150 °C (Fig. 7 (c)) and 200 °C

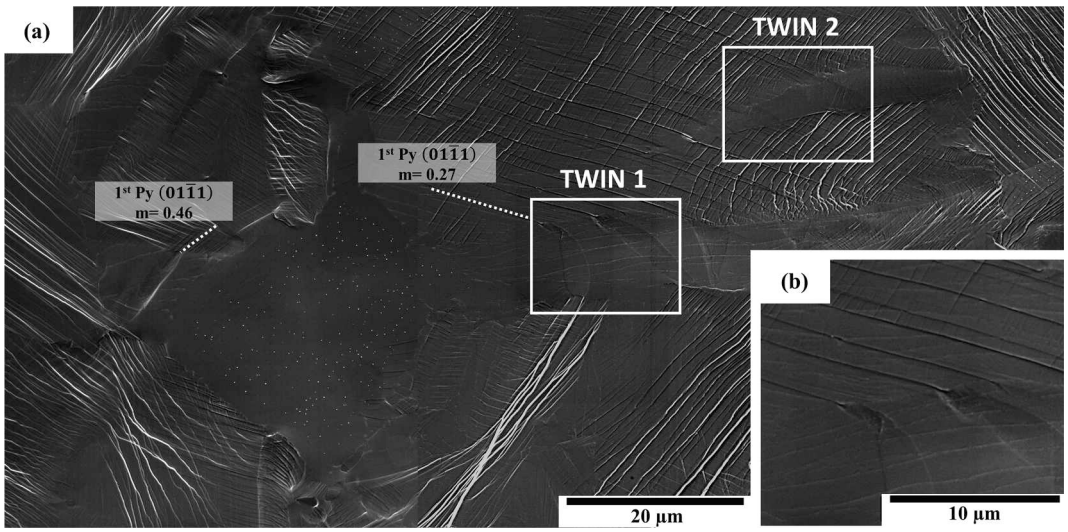

Fig. 9. (a) SE image displaying tensile twins on a hard colony with slip traces and (b) High-resolution SE of slip/twin interaction of hard α_s colonies surrounding a α_p grain after 550 cycles at 150 °C. IPF-LD map of this location shown in Fig. 8.

(Fig. 7 (d)) basal <a> slip was observed in hard orientated grains with a low Schmid factor, below 0.17. Two of these occurrences at the 150 °C specimen are further investigated in section 3.5.

Similar to previous studies, basal and prismatic <a> type of slips are predominant in α_p grains under dwell fatigue conditions in Ti64 [41] and Ti6242 [42], as shown in Fig. 5. Most research reports that dwell fatigue facets were found in grains with their c-axis between 10° and 30° from the loading axis with no presence of twins, neither in grains nor in colonies [7,8]. In this study, slip occurs in grains with their c-axis with declination values of 5° from the loading axis, Fig. 6. Basal slips with Schmid factors below 0.25 were present at 120 °C, 150 °C and 200 °C, and at the lower temperatures occur in agreement with 1st order pyramidal slip, as observed in the example of Fig. 8. Pyramidal <c+a> was reported as an extra mode of deformation accommodation in Ti6242 and Ti834 [38,44–46]. Furthermore, its presence at higher temperature in hard grains has been reported as a way to reduced stress in grain boundaries and therefore reduce dwell fatigue susceptibility at temperatures above 200 °C in Ti6242 [47]. In colonies, deformation by slip happens only with a c-axis declination above 20° while deformation by twinning occurs at c-axis between 10° and 20° as shown for the 150 °C and 200 °C specimens, Fig. 6 (c,d). These results are in accordance with tensile twins observed in Ti64 at room temperature under dwell fatigue conditions [43,44].

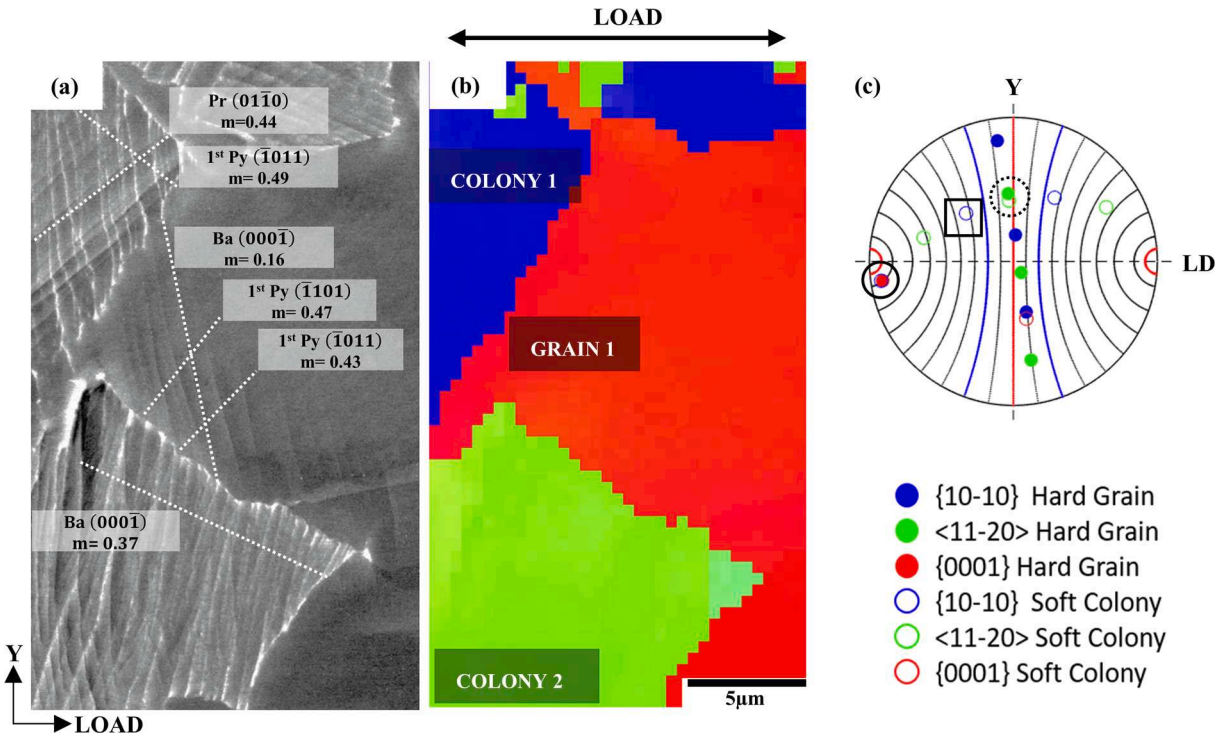

Fig. 10. (a) BSE image with slip traces, (b) IPF-LD orientation map of a hard orientated α_p grain, Grain 1, with <a> basal slip surrounded by soft orientated α_s colonies after 550 cycles at 150 °C and (c) relative pole figure plot regarding the loading direction (horizontal axis) after 550 cycles. Values obtained from the hard grain – Grain 1 (red) and soft colony – Colony 1 (blue) displayed in the IPF-LD orientation map.

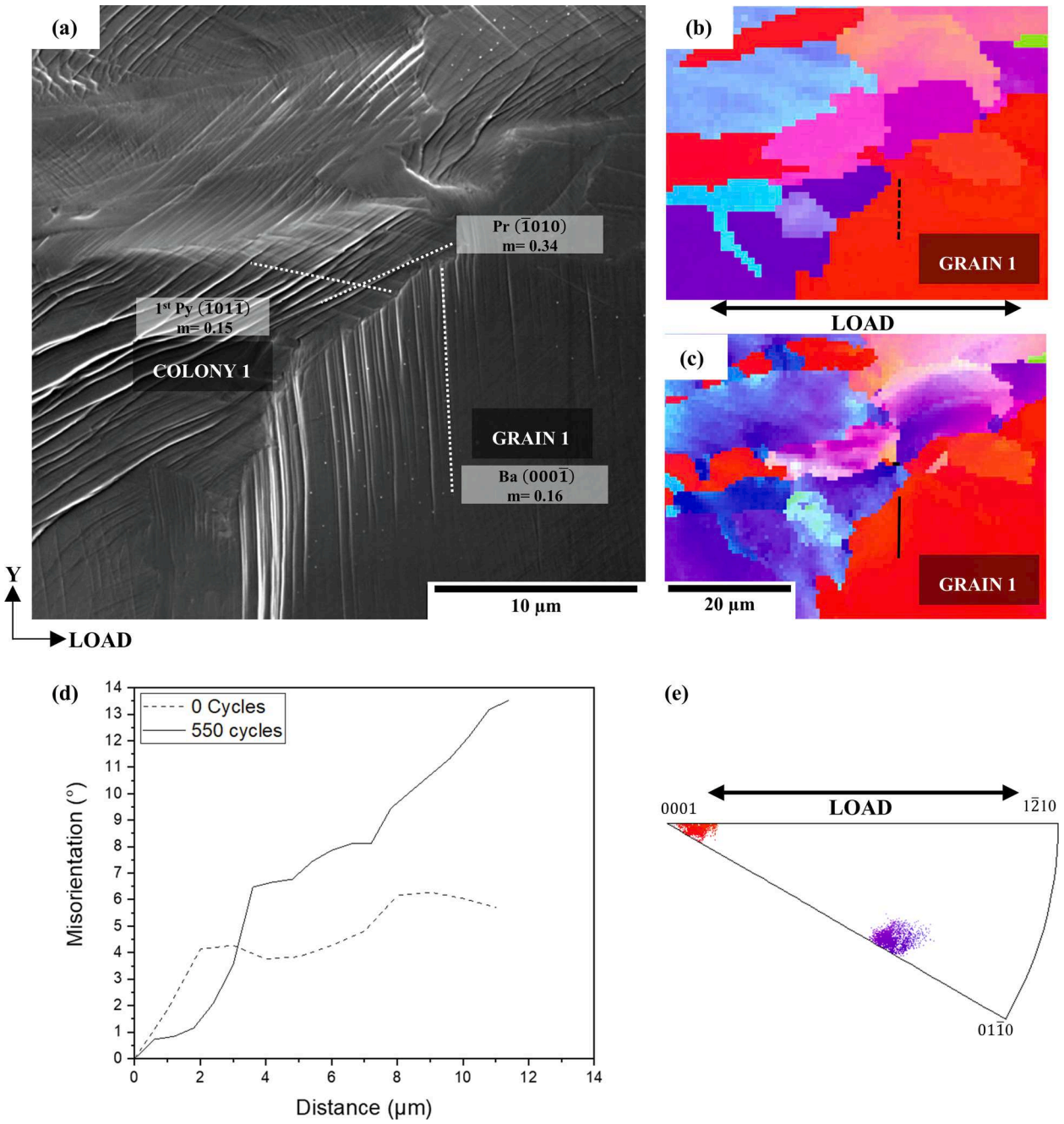

Fig. 11. (a) SE images and IPF-LD orientation maps of basal primary alpha grain with lattice rotation between (b) 0 and (c) 550 cycles at 150 °C. The misorientation profiles highlighted at the Grain I (d) and the inverse pole figure (e) indicates the direction of Grain I regarding the loading direction. Its c-axis is about 8.40° from loading direction.

3.4. Deformation by twining

Tensile twins $\{10\bar{1}2\}\langle 11\bar{2}0 >$ were found in hard-orientated α_s colonies surrounded by soft-orientated colonies, Fig. 8. Twinning was only observed at the higher temperature tests of 150 °C and 200 °C with the twins relatively easy to see after 550 cycles but there was also evidence of twins after 50 cycles but on a much finer scale. Fig. 8 shows the IPF-LD orientation map at 0 cycles Fig. 8 (a) and after 550 cycles Fig. 8 (b) at which twins are observed in the hard colonies. The BSE image (Fig. 8(c)) shows the same region, and it can be noticed that the presence of the tensile twins in conjunction with slip occurring in the neighbouring soft colony.

Accordingly with previous research in CP-Ti [48] and Ti64 [44], the tensile twins observed in Ti834 arises as a result of an incoming slip and its slip band-boundary interaction. Fig. 9 (a, b) shows the presence of the tensile twins in conjunction with slip occurring in the soft colony observed in this investigation. Moreover, it appears that the slip in the soft colony when interacting with the hard colony boundary acts as a nucleation source for twin formation, Fig. 8(b). For the two twin cases in Fig. 9(a) slip in the soft neighbouring colony was 1st order pyramidal slip with relatively high Schmid factor (m = 0.46 and m = 0.27).

Deformation by twinning is presently reported as an operating deformation mechanism under low cycle dwell fatigue conditions in Ti834 at the testing temperatures in hard orientated α_s colonies. No previous evidence of twinning was reported under cycling conditions for Ti834, while tensile twins were recently observed in hard orientated

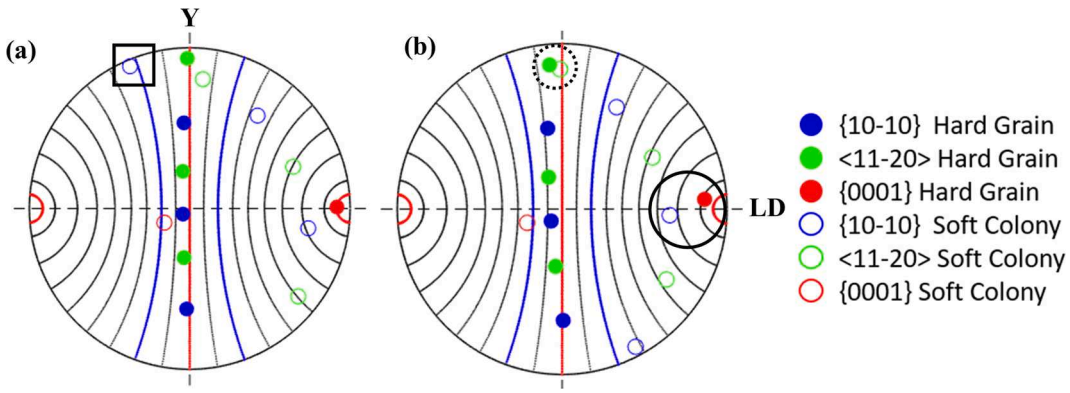

Fig. 12. Relative pole figure plot regarding the loading direction (horizontal axis) after (a) 0 cycles and (b) 550 cycles. Values obtained from the hard grain (red) and soft colony (blue) displayed in Fig. 11.

grains in Ti64 at room temperature [43,44]. Although twins were found here only at 150 °C and 200 °C, full-scale tests done in this same Ti834 compressor disc material have also revealed tensile twins at testing temperature between 80 °C to 250 °C, suggesting that the effect of temperature is negligible at this investigation. Nevertheless, the aluminium content appears to play an important role in twin formation as twins are only observed in α_s colonies. Considering the variation in composition between α_p grains and α_s colonies in this bimodal Ti834 alloy as shown in Table 1, the decrease in 1 wt% Al leads to a 4.71 wt% Al content in α_s colonies compared to the 5.72 wt% Al content in α_p grains. This percentage is close to 4 wt% Al content that was reported as the turning point at which deformation twinning is suppressed during low strain rate room temperature deformation in titanium alloys [49].

Crack initiation sites under dwell fatigue conditions were reported not to be related to the presence of twins in hard α_p grains as reported in Ti64 [43]. In addition, twinning was previously reported to enhance stress relaxation and avoid crack initiation and propagation either by allowing stress relaxation in surrounding hard grains or acting as an obstacle to crack growth [44,50]. Therefore, the presence of twins in hard colonies plays a beneficial role towards reducing dwell fatigue susceptibility.

3.5. Quasi-cleavage facet formation mechanism

Fig. 10 displays one of the aforementioned hard orientated α_p grains with a low Schmid factor, identified as grain 1, surrounded by soft orientated α_s colonies, identified as colony 1 and 2. The basal slip within grain 1 is orientated at 80° to the tensile axis (m = 0.16) but in the same vicinity there are faint slip traces of 1st order pyramidal at 40-50° to the tensile axis (m = 0.43 and m = 0.47), all concentrated at the vicinity of the triple point of grain 1, colony 1, and colony 2. Colony 1 contains a well-defined prismatic <a> slip trace orientated at 40° to the tensile axis (m = 0.44) and a faint 1st order pyramidal slip trace orientated at 40° to the tensile axis (m = 0.49). Colony 2 contains a faint basal slip trace at 25° to the tensile axis (m = 0.37). In both colonies 1 and 2, the slip traces were not parallel to lamellar boundaries and were continuous across the lamellar boundaries.

The individual orientations of Grain 1 and Colony 1 are plotted in Fig. 10 (c) where the circles represent the plane normal, in red for the Basal {0001} planes and in blue for Prismatic $\{10\bar{1}0\}$ planes, and in green the slip directions $< 11\bar{2}0 >$. The load is in the horizontal axis and each curved line represent a 10° disorientation increment from the load direction, the lines coloured in red indicate 5° and 90° from the loading direction, the blue coloured line is at 70°. There is one prismatic plane normal in the soft α_s colony between 60°-70° to the loading direction highlighted with a black square which is equivalent to a prismatic plane at 60°-70° to the normal to the load as claimed by Dunne *et al.* [18] to match the Rogue criteria. Moreover, a Basal {0001} plane in the hard grain that is parallel to a Prismatic $\{10\bar{1}0\}$ plane in the soft colony located at 10° degrees from the loading direction highlighted with a black circle. Additionally, the soft colony and hard grain share a common slip direction $< 11\bar{2}0 >$, highlighted with a dashed black circle,

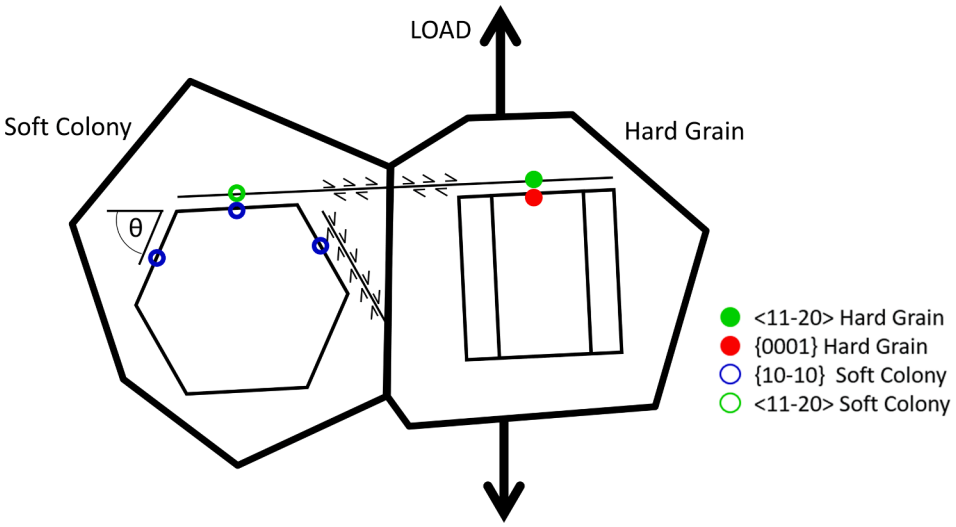

Fig. 13. 2D schematic representation of the rogue grain-colony combination as the grain-colony pair analyses in Figs. 8 and 12.

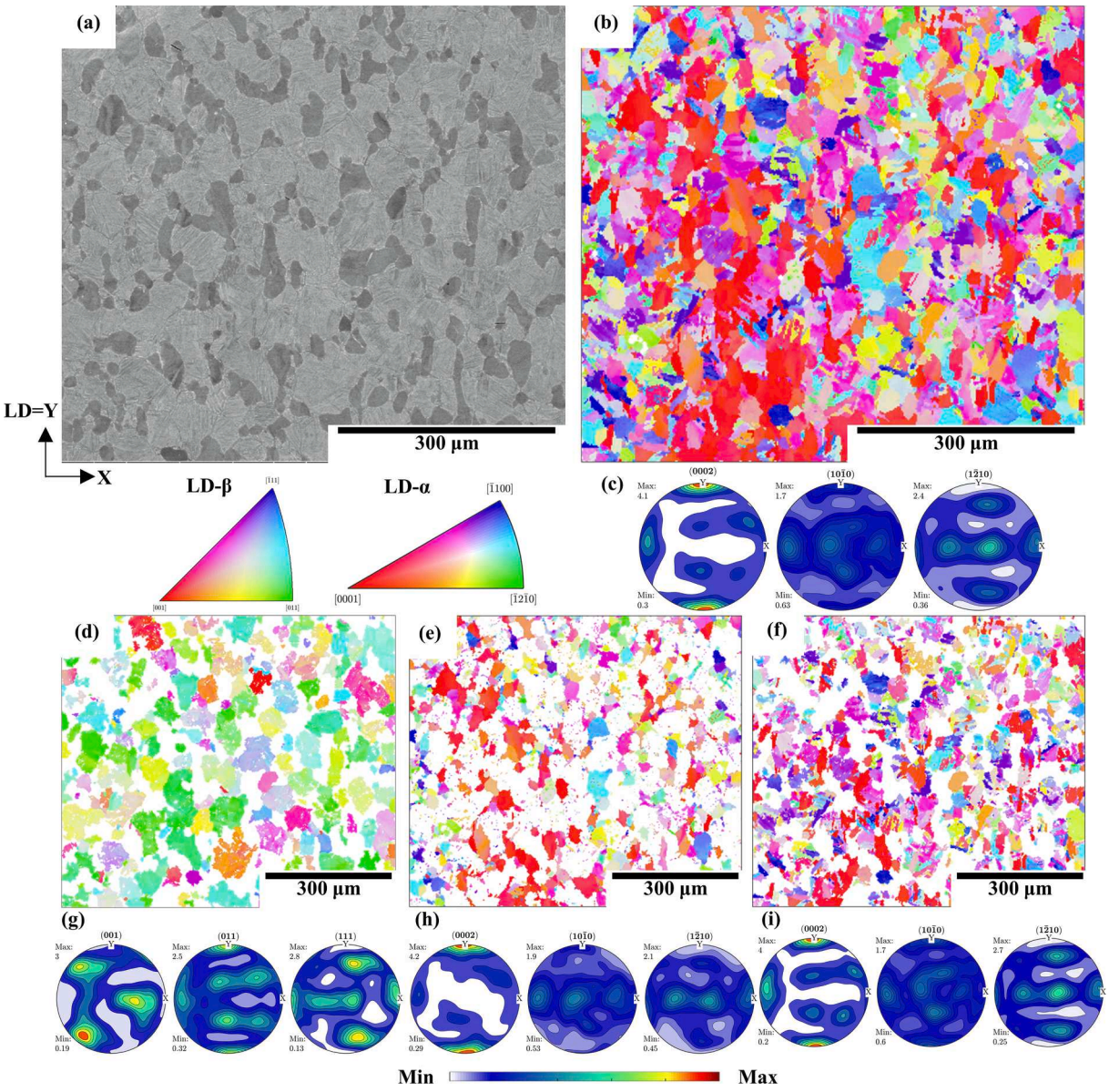

Fig. 14. (a) BSE image, (b) IPF-LD orientation map and (c) pole figures obtained below the main faceted region of a Ti834 cold dwell fatigue tested specimen. Equivalent maps of the (d) reconstructed beta phase, (e) primary alpha grains and (f) secondary alpha colonies are plotted on top of their respective pole figures (g, h,i).

near perpendicular to the loading direction that could lead to slip transfer even though the shear stress in minimum.

A further example of a hard α_p grain displaying a basal <a> type slip (m = 0.16) at 85° from the loading direction neighbouring soft colonies is shown in Fig. 11 (a). Slip traces of Colony 1 are 1st order pyramidal at 11° to the tensile axis, with a very low m value (m = 0.15). The pyramidal slip trace seems to interact with the basal slip on the hard grain, pinning the grain boundary where the basal slip initiates. Wavy sharp lines are observed perpendicular to the pyramidal slip traces, although these matches with a theoretical slip trace for a prismatic <a> trace with a relatively high Schmid factor (m = 0.34), it is not clear whether these lines belong to the lamella boundaries due to their wavy nature or to a slip trace. The IPF maps have confirmed the existence of a lattice rotation. The misorientation angle on grain boundary between soft colony I and hard grain I, decreases from 80° to 76° as cycling increases from 0 to 550 cycles, Fig. 11 (b) and (c), respectively. The cumulative misorientation profiles at Grain I revealed a lattice rotation of up to 8° at the same position from 0 to 550 cycles, Fig. 11(d). Fig. 12 shows the pole figure plot after 50 (a) and 550 (b) cycles at which no such ideal scenario was observed where a 10° mismatch is between basal {0001} and prismatic $\{10\bar{1}0\}$ indicating the presence of a twist boundary.

In both case studies the soft colony and hard grain share a common slip direction <1 1 –2 0>, highlighted with a dashed black circle, near perpendicular to the loading direction that could lead to slip transfer even though the shear stress in minimum. A schematic representation of the rogue colony-grain pair and the planes and direction of slip regarding the loading direction that may lead to quasi cleave formation is proposed in Fig. 13. In agreement with Dunne et al [17,18] and with the initially Stroh's pile up model by Evans and Bache [12] for quasi-cleavage face nucleation, a soft colony is favourably orientated for prismatic <a> slip within a prismatic plane close to an angle θ at about 60°-70° to the loading direction, generating a dislocation pile up in the interphase with the hard grain. Additionally, an extra observation was found in this investigation where the basal and prismatic plane found to be parallel share a common direction which may facilitate slip transfer into the hard grain. Therefore, the present study shows experimental

observations matching the current crystal plasticity models [17,18] for quasi-cleavage facet nucleation at a grain scale where soft-hard pair was observed with a Rogue grain combination as previously done at a macrozone scale [14].

Experimental models and validations so far were mainly focused on equiaxed microstructure [19,22,51] with few research in bimodal microstructures such as the one used in service conditions [23]. Few experimental information was previously used to verify the crystal plasticity models as well as the crystallographic-morphological interaction. Orientation data from faceted regions of Ti6242 microstructure tested under dwell fatigue conditions was previously used at a macrozone scale [9]. In this research, the orientation data obtained at a grain/colony scale agrees with the suppositions made by the crystal plasticity models leading to quasi-cleavage facet nucleation.

3.6. High density rogue region

A cluster of the rogue colony-grain pair of interest was also observed close to the crack initiation site of standard size low cycle dwell fatigue tested specimens from the exact same Ti834 compressor disc material. The texture analysis in the longitudinal cross-section below the fracture surface revealed a cluster consisting mainly of hard grains. The grains belonging to the cluster regions are elongated. The separation between grains and colonies, Fig. 14(e,f) respectively, indicated that the basal nature of the cluster is provided by the grains and reinforced in less degree by colonies, as it can be noticed in the pole figures. While most of grains within this cluster have their c-axis parallel or near parallel to the loading direction (LD) the colonies are about 60° to 70°. While there is a strong variant selection on the colonies generated by the single texture component aligned with LD (Fig. 14 (h,i)) the soft colonies are a pure transformation by the BOR between colonies and the parent beta grains (Fig. 14 (g,i)). As only features with a strict Burgers Orientation Relationship (BOR) are reconstructed, most of the αp grains are missing in the β reconstructed map. However, the αp grain from Pair I was reconstructed indicating a close BOR with the neighbouring parent β grain. This means that a suitably orientated parent β grain by itself can lead to the rogue orientation through specific neighbouring secondary α colonies as well as between a grain-colony pair if the is a near BOR between the αp grain and the parent β grain. This indicates that the presence of rogue pairs is unlikely to be avoided.

4. Conclusions

The deformation behaviour at different temperatures in Ti834 with a bimodal microstructure is studied under dwell fatigue cyclic conditions. The experiments performed using ex-situ EBSD provide evidence of high strain accumulation from early stages in cycling. The analysis was focused on understanding the quasi-cleavage facet formation mechanism and the iteration between soft-hard pairs of α_p grains and α_s colonies. The influence of temperature and texture on the deformation behaviour was discussed:

1. The experiments performed using ex-situ EBSD provide evidence of high strain accumulation from early stages in cycling. A faster creep rate observed for the specimen with a soft texture may suggest that the higher density of soft grains or colonies may enhance creep rate and therefore produce stress relaxation at lower temperatures than the predicted to reduced dwell fatigue sensitivity in Ti834.
2. In this work, Basal <a> slip and Tensile twins $\{10\bar{1}2\}\langle 11\bar{2}0 >$ were observed in α_p grains and α_s colonies respectively orientated with their c-axis relatively close to the loading direction, with declination angles between 5° to 20°. Deformation by twinning is presently reported as an operating deformation mechanism under low cycle dwell fatigue conditions in Ti834 at the testing temperatures in hard orientated α_s colonies despite its high aluminium content.
3. An experimental validation of the findings made by the crystal plasticity model of Dunne et al. [14,18] for quasi-cleavage facet nucleation was obtained at a grain scale by a rogue combination consisting of a soft α_s colony-hard α_p grain pair in this bimodal microstructure displaying Basal <a> slip on hard grains. A high density of rogue pairs was found below fracture surface that appears to be generated by BOR and variant selection triggered by hard orientated macrozones.

Declaration of Competing Interest

The authors declare that they have no known competing financial interests or personal relationships that could have appeared to influence the work reported in this paper.

Acknowledgments

This research is funded by Rolls-Royce Plc. and The Engineering and Physical Science Research Council (UK) through the Centre for Doctoral Training in Advanced Metallic Systems [EP/L016273]. The authors gratefully acknowledge the financial assistance of the National Science Centre Poland [UMO-2015/19/B/ST8/01079].

References

[1] Bache MR. A review of dwell sensitive fatigue in titanium alloys: The role of microstructure, texture and operating conditions. Int J Fatigue 2003;25:1079–87. https://doi.org/10.1016/S0142-1123(03)00145-2.
[2] Bache MR, Cope M, Davies HM, Evans WJ, Harrison G. Dwell sensitive fatigue in a near alpha titanium alloy at ambient temperature. Int J Fatigue 1997;19(93):83–8.
[3] Tympel PO, Lindley TC, Saunders EA, Dixon M, Dye D. Influence of complex LCF and dwell load regimes on fatigue of Ti-6Al-4V. Acta Mater 2016;103:77–88. https://doi.org/10.1016/j.actamat.2015.09.014.
[4] Kassner ME, Kosaka Y, Hall JA. Low-Cycle Dwell-Time Fatigue in Ti-6242, 30; (1999) 2383–89.
[5] Cuddihy MA, Stapleton A, Williams S, Dunne FPE. On cold dwell facet fatigue in titanium alloy aero-engine components. Int J Fatigue 2017;97:177–89. https://doi.org/10.1016/j.ijfatigue.2016.11.034.
[6] Pilchak AL, Williams JC. Observations of facet formation in near-α titanium and comments on the role of hydrogen. Metall Mater Trans A Phys Metall Mater Sci 2011;42:1000–27. https://doi.org/10.1007/s11661-010-0507-9.
[7] Sinha V, Mills MJ, Williams JC. Crystallography of fracture facets in a near-alpha titanium alloy. Metall Mater Trans A Phys Metall Mater Sci 2006;37:2015–26. https://doi.org/10.1007/s11661-006-0144-5.
[8] Sinha V, Mills MJ, Williams JC. Understanding the contributions of normal-fatigue and static loading to the dwell fatigue in a near-alpha titanium alloy. Metall and Mat Trans A 2004;35(10):3141–8.
[9] Sinha V, Spowart JE, Mills MJ, Williams JC. Observations on the faceted initiation site in the dwell-fatigue tested Ti-6242 alloy: Crystallographic orientation and size effects. Metall Mater Trans A Phys Metall Mater Sci 2006;37:1507–18. https://doi.org/10.1007/s11661-006-0095-x.
[10] Germain L, Gey N, Humbert M, Vo P, Jahazi M, Bocher P. Texture heterogeneities induced by subtransus processing of near alpha titanium alloys. Acta Mater 2008; 56:4298–308. https://doi.org/10.1016/j.actamat.2008.04.065.
[11] Stroh AN. The formation of cracks as a result of plastic flow; (1953) 404–14.
[12] Evans WJ, Bache MR. Dwell-sensitive fatigue under biaxial loads in the near-alpha titanium alloy IMI685. Int J Fatigue 1994;16:443–52. https://doi.org/10.1016/0142-1123(94)90194-5.
[13] Hasija V, Ghosh S, Mills MJ, Joseph DS. Deformation and creep modeling in polycrystalline Ti-6Al alloys. Acta Mater 2003;51:4533–49. https://doi.org/10.1016/S1359-6454(03)00289-1.
[14] Dunne FPEE, Rugg D. On the mechanisms of fatigue facet nucleation in titanium alloys. Fatigue Fract Eng Mater Struct 2008;31:949–58. https://doi.org/10.1111/j.1460-2695.2008.01284.x.
[15] Zhang Z, Cuddihy MA, Dunne FPE. On rate-dependent polycrystal deformation: the temperature sensitivity of cold dwell fatigue. Proc R Soc A 2015;471(2181): 20150214.
[16] Zheng Z, Balint DS, Dunne FPE. Discrete dislocation and crystal plasticity analyses of load shedding in polycrystalline titanium alloys. Int J Plast 2016;87:15–31. https://doi.org/10.1016/j.ijplas.2016.08.009.
[17] Dunne FPE, Rugg D, Walker A. Lengthscale-dependent, elastically anisotropic, physically-based hcp crystal plasticity: Application to cold-dwell fatigue in Ti alloys. Int J Plast 2007;23:1061–83. https://doi.org/10.1016/j.ijplas.2006.10.013.
[18] Dunne FPE, Walker A, Rugg D. A systematic study of hcp crystal orientation and morphology effects in polycrystal deformation and fatigue. Proc R Soc A Math Phys Eng Sci 2007;463:1467–89. https://doi.org/10.1098/rspa.2007.1833.
[19] Zhang Z, Cuddihy MA. Dunne FPE. On rate-dependent polycrystal deformation : the temperature sensitivity of cold dwell fatigue Subject Areas; 2015.

[20] Neal DF. Creep fatigue interctions in titanium alloys. In: Sixth World Conf. France: Titan; 1988. p. 175–80.
[21] Engineering Materials, ProcessesTitanium. Berlin, Heidelberg: Springer Berlin Heidelberg; 2007.
[22] Zheng Z, Balint DS, Dunne FPE. Mechanistic basis of temperature-dependent dwell fatigue in titanium alloys. J Mech Phys Solids 2017;107:185–203. https://doi.org/10.1016/j.jmps.2017.07.010.
[23] Zheng Z, Stapleton A, Fox K, Dunne FPE. Understanding thermal alleviation in cold dwell fatigue in titanium alloys. Int J Plast 2018;111:234–52. https://doi.org/10.1016/j.ijplas.2018.07.018.
[24] Shen S, Zhan M, Gao P, Hao W, Dunne FPE, Zheng Z. Microstructural effects on thermal-mechanical alleviation of cold dwell fatigue in titanium alloys. Crystals 2022;12:1–9. https://doi.org/10.3390/cryst12020208.
[25] Leyens C, Peters M. Titanium and titanium alloys: fundamentals and applications. Weinheim.: Wiley-VCH; 2003.
[26] Hémery S, Villechaise P. Comparison of slip system activation in Ti-6Al-2Sn-4Zr-2Mo and Ti-6Al-2Sn-4Zr-6Mo under tensile, fatigue and dwell-fatigue loadings. Mater Sci Eng A 2017;697:177–83. https://doi.org/10.1016/j.msea.2017.05.021.
[27] Anahid M, Samal MK, Ghosh S. Dwell fatigue crack nucleation model based on crystal plasticity finite element simulations of polycrystalline titanium alloys. J Mech Phys Solids 2011;59:2157–76. https://doi.org/10.1016/j.jmps.2011.05.003.
[28] Lunt D, Thomas R, Atkinson MD, Smith A, Sandala R, da Fonseca JQ, et al. Understanding the role of local texture variation on slip activity in a two-phase titanium alloy. Acta Mater 2021;216:117111. https://doi.org/10.1016/j.actamat.2021.117111.
[29] Gey N, Bocher P, Uta E, Germain L, Humbert M. Texture and microtexture variations in a near-α titanium forged disk of bimodal microstructure. Acta Mater 2012;60(6-7):2647–55.
[30] Pilchak AL, Szczepanski CJ, Shaffer JA, Salem AA, Semiatin SL. Characterization of microstructure, texture, and microtexture in near-alpha titanium mill products, in. Metall Mater Trans A Phys Metall Mater Sci 2013;44(11):4881–90.
[31] Uta E, Gey N, Bocher P, Humbert M, Gilgert J. Texture heterogeneities in αp/αstitanium forging analysed by EBSD-Relation to fatigue crack propagation. J Microsc 2009;233(3):451–9.
[32] Uta E, Gey N, Bocher P, Humbert M, Gilgert J. Texture heterogeneities in αp/αs titanium forging analysed by EBSD-Relation to fatigue crack propagation. J Microsc 2009;233:451–9. https://doi.org/10.1111/j.1365-2818.2009.03141.x.
[33] Everaerts J, Gontcharov D, Verlinden B, Wevers M. The influence of load holds on the fatigue behaviour of drawn Ti-6Al-4V wires. Int J Fatigue 2017;98:203–11. https://doi.org/10.1016/j.ijfatigue.2017.01.043.
[34] Sackett E, Germain L, Bache M. Crystal plasticity, fatigue crack initiation and fatigue performance of advanced titanium alloys. Int J Fatigue 2007;29(9-11):2015–21.
[35] Badea L, Surand M, Ruau J, Viguier B, Badea L, Surand M, et al. Creep behavior of Ti-6Al-4V from 450°C to 600°C. Univ Polytech Bucharest Sci Bull 2014;76(1):185–96.
[36] Li W, Chen Z, Liu J, Wang Q, Sui G. Effect of texture on anisotropy at 600 °C in a near-α titanium alloy Ti60 plate. Mater Sci Eng A 2017;688:322–9. https://doi.org/10.1016/j.msea.2017.01.098.
[37] Barkia B, Doquet V, Couzinié JP, Guillot I. Room-temperature creep and stress relaxation in commercial purity titanium-Influence of the oxygen and hydrogen contents on incubation phenomena and aging-induced rejuvenation of the creep potential. Mater Sci Eng A 2015;624:79–89. https://doi.org/10.1016/j.msea.2014.11.073.
[38] Bridier F, Villechaise P, Mendez J. Analysis of the different slip systems activated by tension in a a / b titanium alloy in relation with local crystallographic orientation 2005;53:555–67. https://doi.org/10.1016/j.actamat.2004.09.040.
[39] Hémery S, Villechaise P. On the influence of ageing on the onset of plastic slip in Ti-6Al-4V at room temperature: Insight on dwell fatigue behavior. Scr Mater 2017;130:157–60. https://doi.org/10.1016/j.scriptamat.2016.11.042.
[40] Littlewood PD, Wilkinson AJ. Local deformation patterns in Ti-6Al-4V under tensile, fatigue and dwell fatigue loading. Int J Fatigue 2012;43:111–9. https://doi.org/10.1016/j.ijfatigue.2012.03.001.
[41] Lavogiez C, Hémery S, Villechaise P. Analysis of deformation mechanisms operating under fatigue and dwell-fatigue loadings in an α/β titanium alloy. Int J Fatigue 2020;131:105341.
[42] Hémery S, Guéguen M, Villechaise P. Mechanical study of crystalline orientation distribution in Ti-6Al-4V : An assessment of micro-texture induced load partitioning. Mater Des 2018;137:22–32. https://doi.org/10.1016/j.matdes.2017.10.011.
[43] Lavogiez C, Hémery S, Villechaise P. Analysis of deformation mechanisms operating under fatigue and dwell- fatigue loadings in an α / β titanium alloy. Int J Fatigue 2020;131:105341. https://doi.org/10.1016/j.ijfatigue.2019.105341.
[44] Lavogiez C, Hémery S, Villechaise P. Concurrent operation of ⟨c + a⟩ slip and twinning under cyclic loading of Ti-6Al-4V. Scr Mater 2018;157:30–3. https://doi.org/10.1016/j.scriptamat.2018.07.033.
[45] Joseph S, Joseph K, Lindley TC, Dye D. On the dislocation mechanisms leading to cracking in dwell fatigue of a near-alpha titanium alloy; (2019). http://arxiv.org/abs/1905.11714.
[46] Baxter GJ, Rainforth WM, Grabowski L. TEM observations of fatigue damage accumulation at the surface of the near alpha titanium alloy IMI 834. Acta Mater 1996;44:3453–63. https://doi.org/10.1016/1359-6454(96)00024-9.
[47] Ready AJ, Haynes PD, Grabowski B, Rugg D, Sutton AP. The role of molybdenum in suppressing cold dwell fatigue in titanium alloys, in. Proc R Soc A Math Phys Eng Sci 2017;473(2203):20170189.
[48] Wang L, Yang Y, Eisenlohr P, Bieler TR, Crimp MA, Mason DE. Twin nucleation by slip transfer across grain boundaries in commercial purity titanium. Metall Mater Trans A Phys Metall Mater Sci 2010;41:421–30. https://doi.org/10.1007/s11661-009-0097-6.
[49] Fitzner A, Thomas M, Quinta J, Zhang S, Kelleher J, Preuss M et al., The effect of aluminium on deformation and twinning in alpha titanium : the ND case; (2016) 1051–56.
[50] Ma Y, Xue Q, Wang H, Huang S, Qiu J, Feng X, et al. Deformation twinning in fatigue crack tip plastic zone of Ti-6Al-4V alloy with Widmanstatten microstructure. Mater Charact 2017;132:338–47. https://doi.org/10.1016/j.matchar.2017.08.029.
[51] Ozturk D, Pilchak AL, Ghosh S. Experimentally validated dwell and cyclic fatigue crack nucleation model for α–titanium alloys. Scr Mater 2017;127:15–8. https://doi.org/10.1016/j.scriptamat.2016.08.031.